

# Direct Calculation of the Turbulent Dissipation Efficiency in Anelastic Convection

Kaloyan Penev, Joseph Barranco, Dimitar Sasselov

Kaloyan Penev<sup>a</sup>, Joseph Barranco<sup>b</sup>, Dimitar Sasselov<sup>c</sup>

<sup>a</sup>60 Garden St., M.S. 10, Cambridge, MA 02138

<sup>b</sup>1600 Holloway Avenue, San Francisco, CA 94132-4163

<sup>c</sup>60 Garden St., M.S. 16, Cambridge, MA 02138

---

## Abstract

The current understanding of the turbulent dissipation in stellar convective zones is based on the assumption that the turbulence follows Kolmogorov scaling. This assumption is valid for some cases in which the time frequency of the external shear is high (e.g. solar p-modes). However, for many cases of astrophysical interest (e.g. binary orbits, stellar pulsations e.t.c.) the timescales of interest lie outside the regime of applicability of Kolmogorov scaling. We present direct calculations of the dissipation efficiency of the turbulent convective flow in this regime using simulations of anelastic convection with external forcing. We show that the effects of the turbulent flow are well represented by an effective viscosity coefficient and we provide the values of the effective viscosity as a function of the perturbation frequency. In addition we justify a perturbative method for finding the effective viscosity (proposed by Goodman & Oh (1997)) that can be applied to actual simulations of the surface convective zones of stars.

*Key words:* Hydrodynamics, Anelastic approximation, Stratified flows, Shear flows, Spectral methods, Convection, Turbulence, Turbulent dissipation, Effective Viscosity

---

## 1. Introduction

For stars with surface convection, turbulent dissipation in the convective zone is believed to be the dominant mechanism responsible for the conversion of mechanical energy of tides, stellar oscillations and stellar pulsations to heat. Thus this is the mechanism believed to determine the rates of tidal synchronization and circularization (Zahn, 1966, 1989), the amplitudes of stellar  $p$  and  $g$  modes (Goldreich & Keeley, 1977; Goldreich & Kumar, 1988; Goldreich et al., 1994), and the instability of stars to pulsations (Gonczi, 1982).

The simplest approach to estimating the dissipation efficiency of the turbulent convection is to assume that the turbulence is homogeneous and isotropic and its interaction with external shear is only local. In that case we can define an effective viscosity coefficient which will capture the effects

due to the turbulent flow. The question then is how to find the value of this coefficient.

Currently two prescriptions based on the assumption of Kolmogorov cascade exist for estimating this coefficient as a function of the time period of the external shear ( $T$ ).

Zahn (1966, 1989) proposes that, the effective viscosity should scale linearly with the fraction of a turn eddies manage to complete in half a perturbation period:

$$\nu = \nu_{max} \min \left[ \left( \frac{T}{2\tau} \right), 1 \right]. \quad (1)$$

On the other hand, Goldreich & Nicholson (1977) and Goldreich & Keeley (1977), argue that eddies with turnover times bigger than  $T/2\pi$  will not contribute to the dissipation. Then Kolmogorov scaling predicts:

$$\nu = \nu_{max} \min \left[ \left( \frac{T}{2\pi\tau} \right)^2, 1 \right] \quad (2)$$

Zahn's more efficient dissipation seems to be in better agreement with observations of tidal circularization times for binaries containing a giant star (Verbunt & Phinney, 1995), the location of the red edge of the Cepheid instability strip (Gonczi, 1982), and even this more efficient prescription might be insufficient to explain the main sequence circularization of binary stars in clusters (Meibom & Mathieu, 2005).

However, Goldreich & Keeley (1977), Goldreich & Kumar (1988) and Goldreich et al. (1994), successfully used the less efficient dissipation to develop a theory for the damping of the solar  $p$ -modes. In this case the more effective dissipation would require dramatic changes in the excitation mechanism in order to explain the observed amplitudes.

Finally, Goodman & Oh (1997) calculated a lowest order expansion of the effective viscosity, which when applied to Kolmogorov turbulence predicts a result closer to the less efficient Goldreich & Nicholson viscosity. While this gives a firmer theoretical foundation for the less efficient prescription it does not help with the observational problem of insufficient dissipation in the case of tides and stellar pulsations.

A possible resolution of this problem is suggested by the fact that the successful applications of the two prescriptions correspond to very different perturbation periods. The Zahn (1966, 1989) scaling seems to work well for periods of order days, and the Goldreich and collaborators quadratic scaling seems to apply to periods of order minutes. This distinction is important, because in stars with surface convection Kolmogorov scaling predicts that the eddies with turnover times of several minutes would have typical sizes that are very small compared to the local pressure scale height and any other external length scales. On the other hand turnover times of days correspond to eddies with typical sizes comparable or larger than the local pressure scale height. In this case Kolmogorov scaling is not expected to apply.

The flow seen in 2D and 3D simulations of stellar convection is very different from a Kolmogorov cascade (Sofia & Chan, 1984; Stein & Nordlund, 1989; Malagoli et al., 1990). There are two important distinctions. The first

is that the velocity power spectrum is much flatter in the simulations than Kolmogorov, and so one expects to find a slower loss of dissipation efficiency with increased frequency of the external shear, as long as the external shear has a period that corresponds to eddy turnover times too long to fall in the inertial subrange of Kolmogorov turbulence. The second is that the flow is no longer isotropic and hence the effective viscosity should be a tensor, rather than a scalar.

As a first attempt to explore this possibility Penev et al. (2007, 2008b) adapted the Goodman & Oh (1997) perturbative calculation to the Robinson et al. (2003) numerical model of stellar convection and found a highly asymmetric effective viscosity that scaled linearly with the period of the external shear. However, their perturbative calculation is applicable only as long as the forcing period  $T$  is small compared to the turnover time of the largest eddies. In particular the perturbative treatment is not able to provide the maximum value the effective viscosity reaches and the frequency at which it reaches it, which is of great importance in calculating tidal interactions and dissipation of pulsations.

In this article we use the Penev et al. (2008a) spectral anelastic code to perform a direct calculation of the turbulent dissipation in a convective zone, by introducing external shear as an extra body force in the fluid equations. The goal is to investigate the applicability of effective viscosity as an approximation to the actual turbulent dissipation and the reliability of the Goodman & Oh (1997) formalism.

## 2. Simulations

### 2.1. Steady State Convection

The details of the numerical simulation and the equations evolved are presented in Penev et al. (2008a). We are simulating a rectangular box with impenetrable, constant temperature top and bottom boundaries (the  $\hat{z}$  velocity vanishes and the temperature is held at some constant value at the top and bottom walls of the box). The choice of parameters for our flow and the motivation for this choice is presented in section 4.1 of that article. Here we briefly remind those parameters:

$L_x = L_y = L_z = 4$	The physical dimensions of the convective box.
$N_x = N_y = N_z = 128$	resolution in each direction
$p_{top} = 1.0 \times 10^5$	background pressure at the top of the box
$g = 2.74$	gravitational acceleration, in $-\hat{z}$ direction
$C_p = 0.21$	Specific heat at constant pressure of the fluid
$R = 8.317 \times 10^{-2}$	ideal gas constant of the fluid
$T_{low} = 10.0$	The temperature at the top boundary of the box
$T_{high} = 62.37$	The temperature at the bottom boundary of the box

In addition, we need to specify a height dependent heat diffusion coefficient ( $\kappa$ ), which we have plotted in fig. 1.

We initialize the box with random entropy fluctuations and let it evolve with time until a steady state is reached. The criteria we used for concluding

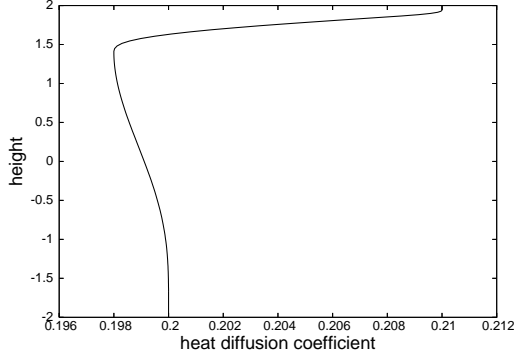


Figure 1: The height dependent heat diffusion coefficient

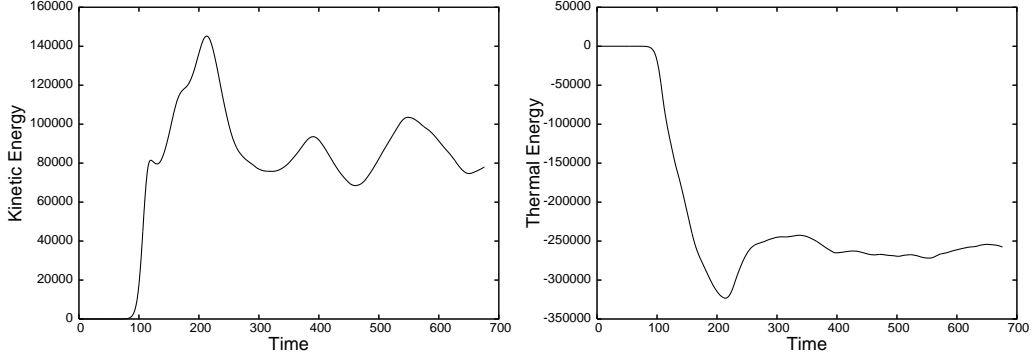


Figure 2: Kinetic (left) and thermal (right) energy content of the convective box used as one of the criteria for having reached a steady state. We decided steady state was reached for times greater than 400.

a steady state has been reached were that the kinetic and thermal energies should stop drifting systematically, and only exhibit oscillations at the approximate convective turnover time (see fig. 2), and that the spatial spectra of the velocity and potential temperature remain constant to within a few percent. The steady state Fourier spatial and time spectra are presented in fig. 3.

## 2.2. External Forcing

After steady state has been reached we introduce external forcing ( $f$ ) in the form of a position and time dependent gravitational acceleration. The simplest form of forcing to interpret was height dependent horizontal forcing. Vertical forcing is easy enough to introduce but the analysis would have to deal with the impenetrable top and bottom boundary walls. Those walls are an issue even for the horizontally forced box, so we chose a forcing profile that is close to zero near those boundaries. The particular shape we chose for our forcing profile was a Gaussian with a maximum at the center of the box and a standard deviation of 0.5. The time dependence was a simple cosine. So, in short, the anelastic momentum equation that we evolved was:

$$\frac{\partial \mathbf{v}}{\partial t} = \mathbf{v} \times \boldsymbol{\omega} - \nabla \tilde{h} + \frac{\tilde{\theta}}{\bar{\theta}} g \hat{\mathbf{z}} + \mathbf{f} \quad (3)$$

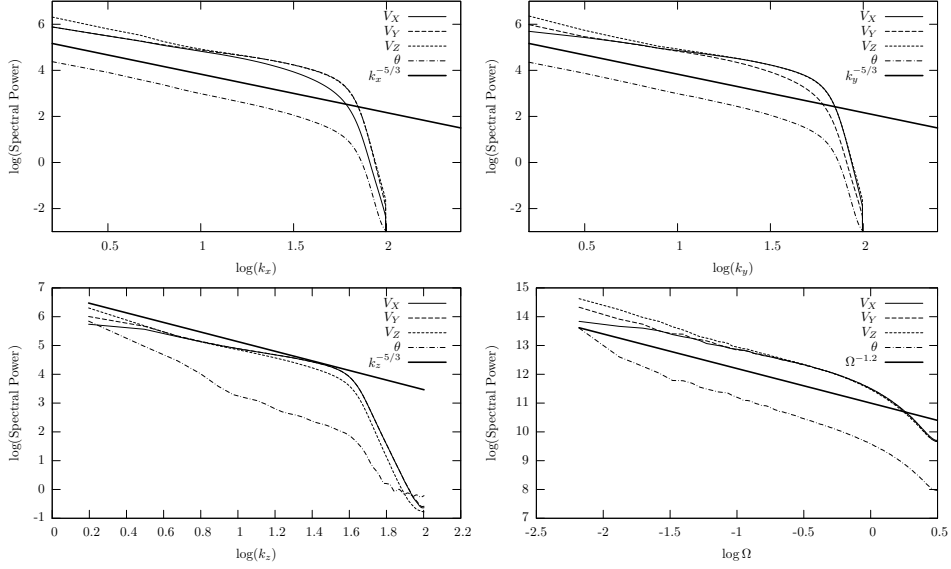


Figure 3: The (x: top left, y: top right, z: bottom left, time: bottom right) spectra of the 3 velocity components and the potential temperature. The thick line in the spatial spectra plots corresponds to Kolmogorov scaling ( $E_k \propto k^{-5/3}$ ). The thick line in the time spectra plot corresponds to the scaling we find for the effective viscosity using the Goodman & Oh (1997) applied on the steady state convection (see eq. 5).

Where quantities with tilde represent anelastic perturbations to the background quantities (denoted by an over bar),  $\mathbf{v}$  is the velocity vector,  $\tilde{h} \equiv \tilde{p}/\bar{\rho} + \mathbf{v}^2/2$  is the enthalpy,  $\tilde{\theta}$  is the perturbation to the background potential temperature  $\bar{\theta} = \bar{T} (p_0/\bar{p})^{R/C_p}$  and  $\mathbf{f}$  is the external forcing given by:

$$\mathbf{f}(z, t) = f_0 e^{-2z^2} \cos\left(\frac{2\pi t}{T}\right) \hat{x} \quad (4)$$

Clearly the amplitude of the forced velocity will be  $\approx f_0 T/2\pi$ , so we evolved a number of flows with different periods and the same  $f_0 T$ . That way the shear created by the external forcing was similar for all the flows in the set. We evolved two such sets one at 20 different frequencies and one at 11 for a total of 31 different cases of forcing. Table 1 summarizes the runs and the respective number of time steps that we ran each case for. Notice that the weak forcing cases required a lot more time steps in order to average out the turbulent noise and allow us to detect the systematic energy dissipation.

For the strong forcing case we expect the maximal central velocities to reach  $\max v_x = 1/2\pi \approx 0.16$ , and for the weak forcing  $\max v_x = 0.15/2\pi \approx 0.024$ . For comparison in our convective box the speed of sound varies between 1.2 at the top of the box and 2.9 at the bottom and the typical r.m.s. velocity is between 0.02 and 0.04 (see fig. 4), except near the boundaries of the box where the collision of the vertical flow with the impenetrable boundaries results in higher horizontal velocities.

In the case of tides in binary stellar systems, the velocities excited by the external forcing are small compared to the typical convective velocities, however, performing numerical simulations with forcing small enough to ensure that this is the case will be prohibitive in terms of computational time,

Strong Forcing				Weak Forcing			
$T$	$f_0$	number time steps	saving one time step out of every	$T$	$f_0$	number time steps	saving one time step out of every
300	1/300	120000	10	200	0.15/200	420000	10
250	1/250	150000	10	150	0.15/150	280000	50
225	1/225	135000	10	140	0.15/140	168000	10
200	1/200	60000	10	120	0.15/120	240000	10
190	1/190	133000	10	110	0.15/110	220000	10
180	1/180	144000	10	100	0.15/100	180000	10
170	1/170	136000	10	90	0.15/90	189000	10
160	1/160	144000	10	75	0.15/75	180000	10
150	1/150	60000	50	60	0.15/60	186000	10
110	1/110	66000	10	50	0.15/50	185000	50
100	1/100	60000	50	30	0.15/30	180000	10
90	1/90	63000	10				
75	1/75	60000	50				
60	1/60	60000	10				
55	1/55	60500	10				
50	1/50	60000	50				
45	1/45	63000	10				
40	1/40	60000	10				
30	1/30	60000	50				
10	1/10	60000	50				

Table 1: The forcing amplitude-period combinations for which simulations were run and the number of time steps simulated in each case.

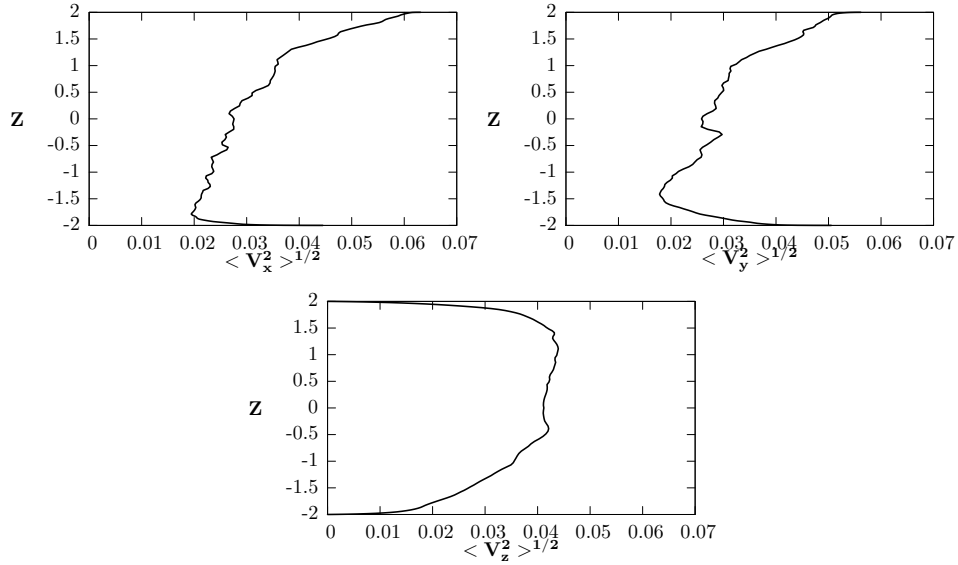


Figure 4: The typical steady state r.m.s. velocities ( $v_x$  top left,  $v_y$  top right,  $v_z$  bottom).

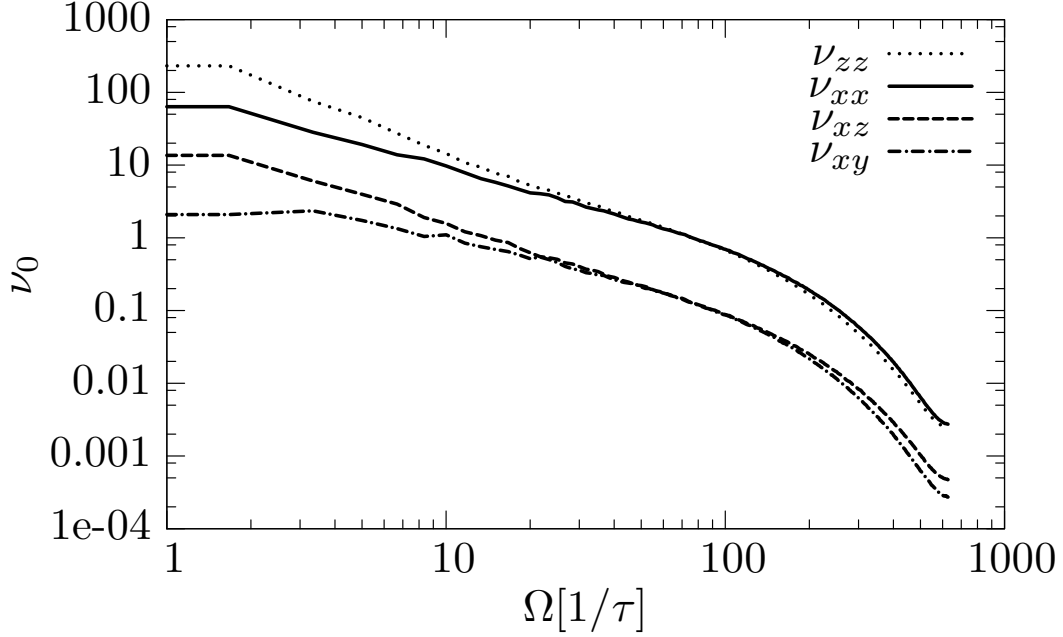


Figure 5: The four independent components of the viscosity tensor estimated using the perturbative approach of Goodman & Oh (1997).

because it will require simulations for excessive number of time steps to make sure the dissipation is noticeable among the fluctuations due to turbulence (see section 3.2).

### 3. Results

#### 3.1. Perturbative Calculation

The obvious first step is to apply the Goodman & Oh (1997) perturbative calculation, as modified in Penev et al. (2007) and Penev et al. (2008b) to account for density stratification and the discrete sampling, to the steady state flow without any forcing. The details of that calculation were presented in Penev et al. (2008a) section 5.2. We include here again the components of the effective viscosity tensor this calculation predicted in fig. 5. The figure contains only four curves (rather than nine), since by assumption the viscosity tensor produced by this method is symmetric, and also physically we expect no difference between the  $\hat{x}$  direction and the  $\hat{y}$  direction in our simulations, so we average the corresponding viscosity components together and only four independent components remain.

The approximate scaling with frequency of the volume average effective viscosity we observe is roughly the same for all four components:

$$\nu \propto \Omega^{-1.2} \quad (5)$$

#### 3.2. Direct Calculation

To simplify the discussion we define upfront the following quantities:

$$C(z) = \sum_{i,j,w} v_x(x_i, y_j, z, t_w) \cos\left(\frac{2\pi t_w}{T}\right) \quad (6)$$

$$S(z) = \sum_{i,j,w} v_x(x_i, y_j, z, t_w) \sin\left(\frac{2\pi t_w}{T}\right) \quad (7)$$

Where  $x_i$  and  $y_j$  are the locations of the  $x$  and  $y$  collocation grid points where we have values for the velocity and  $t_w$  are the times at which we have them. We evaluate the sum over an integer number of forcing periods  $T$ .

### 3.2.1. Fitting the Depth Dependence

We would like to explore the applicability of the effective viscosity framework to the problem of turbulent dissipation. We would like to show that substituting the turbulent flow with a simple viscosity is able to capture not only the total amount of energy dissipated, but also the height dependence of this dissipation. In other words we would like to show that the work per unit mass done by the forcing on the flow at each depth:

$$W_{turb}(z) \equiv f_0 e^{-2z^2} C(z) \quad (8)$$

matches the energy that would be transported and dissipated out of that depth by an assumed effective viscosity:

$$W_{visc}(z) \equiv \nu(z) [C(z)C''(z) + S(z)S''(z)] + \quad (9)$$

$$+ \left( \nu'(z) + \frac{d \log \bar{\rho}}{dz} \nu(z) \right) [C(z)C'(z) + S(z)S'(z)] \quad (10)$$

Where primes denote derivatives with respect to  $z$  and  $\bar{\rho}$  is the background density profile. Note that this is not simply a conservation of energy requirement. We want to see if the transport of energy is captured by the viscosity as well.

Since we allow the viscosity to depend on depth we can always match  $W_{turb}(z)$  to  $W_{visc}(z)$ . However, we use a pre-determined function of depth up to a normalization constant for the effective viscosity, namely:

$$\nu = \nu_0 < v_z^2 >^{1/2} H_p \quad (11)$$

Where  $H_p$  is the pressure scale height. This way we have only one free constant ( $\nu_0$ ) that we can vary in order to match the two rates. On dimensional grounds the turbulent viscosity must scale like the relevant velocity and length scales in the problem. Clearly the relevant velocity scale is the convective velocity and we use  $H_p$  as the length scale in keeping with mixing length theory, where it is assumed that the mixing length will be proportional to the local pressure scale height. One could argue that we should then include the mixing length parameter ( $\alpha$ ), but that simply gets absorbed into the definition of  $\nu_0$ , and we note that it is reasonable to expect that the value of  $\nu_0$  will scale as the mixing length parameter of the convective region. In fact this is seen to be the case by comparing our perturbative calculation results to those of Penev et al. (2008b) (see sec. 4).

A slightly modified version of eq. 11 ( $\nu \propto 1/3 < v^2 >^{1/2} H_p$ ) has been assumed in all previous effective viscosity applications (Zahn, 1966, 1989; Goldreich & Keeley, 1977; Goldreich & Kumar, 1988; Goldreich et al., 1994).

Substituting  $\langle v_z^2 \rangle^{1/2}$  for  $1/3 \langle v^2 \rangle^{1/2}$  is done because we do not expect the effective viscosity to be isotropic and hence we should not be using the total turbulent velocity, but rather, in our particular case of  $\hat{z}$  shear, its  $\hat{z}$  component. In practice this distinction makes little difference since as we can see from fig. 4 away from the boundaries all components of the velocity behave alike, except for the fact that  $v_z$  tends to be larger, which just leads to a smaller value of the normalization constant  $\nu_0$ .

We find the value of  $\nu_0$  by least squares fitting of  $W_{visc}$  to  $W_{turb}$ . Clearly the presence of the turbulence will cause random fluctuations in the velocity profile which should average out if we combine a large enough number of time steps in evaluating the quantities  $C(z)$  and  $S(z)$  of eq. 6 and 7. These fluctuations are highly amplified when we estimate second derivatives of the  $C(z)$  and  $S(z)$  quantities, so  $W_{visc}$  suffers much more than  $W_{turb}$ . Some representative fitted curves are shown in fig. 6 and 7.

We see that for all but one case the two curves match closely which shows that the effective viscosity assumption captures the effects of turbulent dissipation to a good degree. The  $T = 10$  curves for the strong forcing case do not match well at all. The bad fit is due to the fact that if there is any dissipation present it is undetectable from within the turbulent noise.

### 3.2.2. Matching Deposited to Dissipated Power

An alternative way to get a value for the scaling constant  $\nu_0$  is to equate the overall power deposited into the box by the external forcing:

$$\dot{\epsilon}_{ext} = \int_{-Lz/2}^{Lz/2} \bar{\rho}(z) W_{turb}(z) dz \quad (12)$$

to the value that the effective viscosity dissipates out of the box:

$$\dot{\epsilon}_{visc} = \int_{-Lz/2}^{Lz/2} \bar{\rho}(z) \widetilde{W}_{visc}(z) dz \quad (13)$$

Where we have defined  $\widetilde{W}_{visc}(z) \equiv \nu(z) [C'^2(z) + S'^2(z)]$ .

Note that these two quantities do not have the same depth dependence, only their integrals over the entire box must match. The reason for this is that viscous forces redistribute the energy in the box as well as dissipate it. So we cannot use these quantities to examine the applicability of the effective viscosity assumption, but because evaluating  $\widetilde{W}_{visc}(z)$  requires only first derivatives of the  $S(z)$  and  $C(z)$  quantities it suffers significantly less from the turbulent noise than  $W_{visc}(z)$  from section 3.2.1.

Typical plots of the depth dependence of  $\widetilde{W}_{visc}$  for the weak and strong forcing cases are shown in fig. 8 and 9. The depth dependence of  $W_{turb}$  for the same forcing periods was already plotted as the solid curves in fig. 6 and 7.

### 3.3. Comparison Between the Perturbative and Direct Calculation

We compare the Goodman & Oh (1997) based perturbative estimate of the  $x, z$  viscosity coefficient :  $\nu_{xz}$  to the directly calculated effective viscosity obtained by the procedures of sec. 3.2.1 and 3.2.2 in fig. 10.

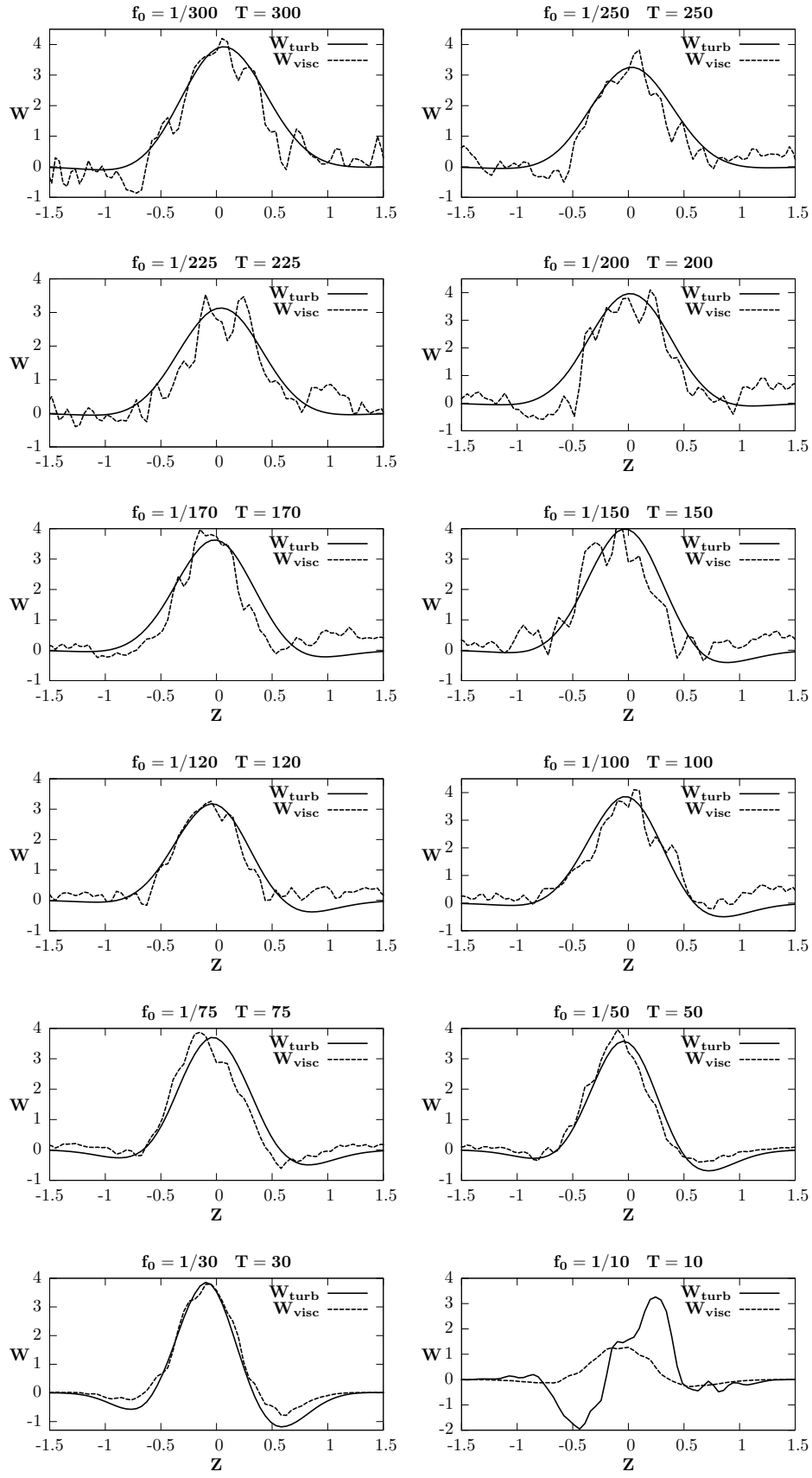


Figure 6: The least squares fit between  $W_{turb}$  (solid curves) and  $W_{visc}$  (dashed curves) for a representative sample of the strong forcing cases.

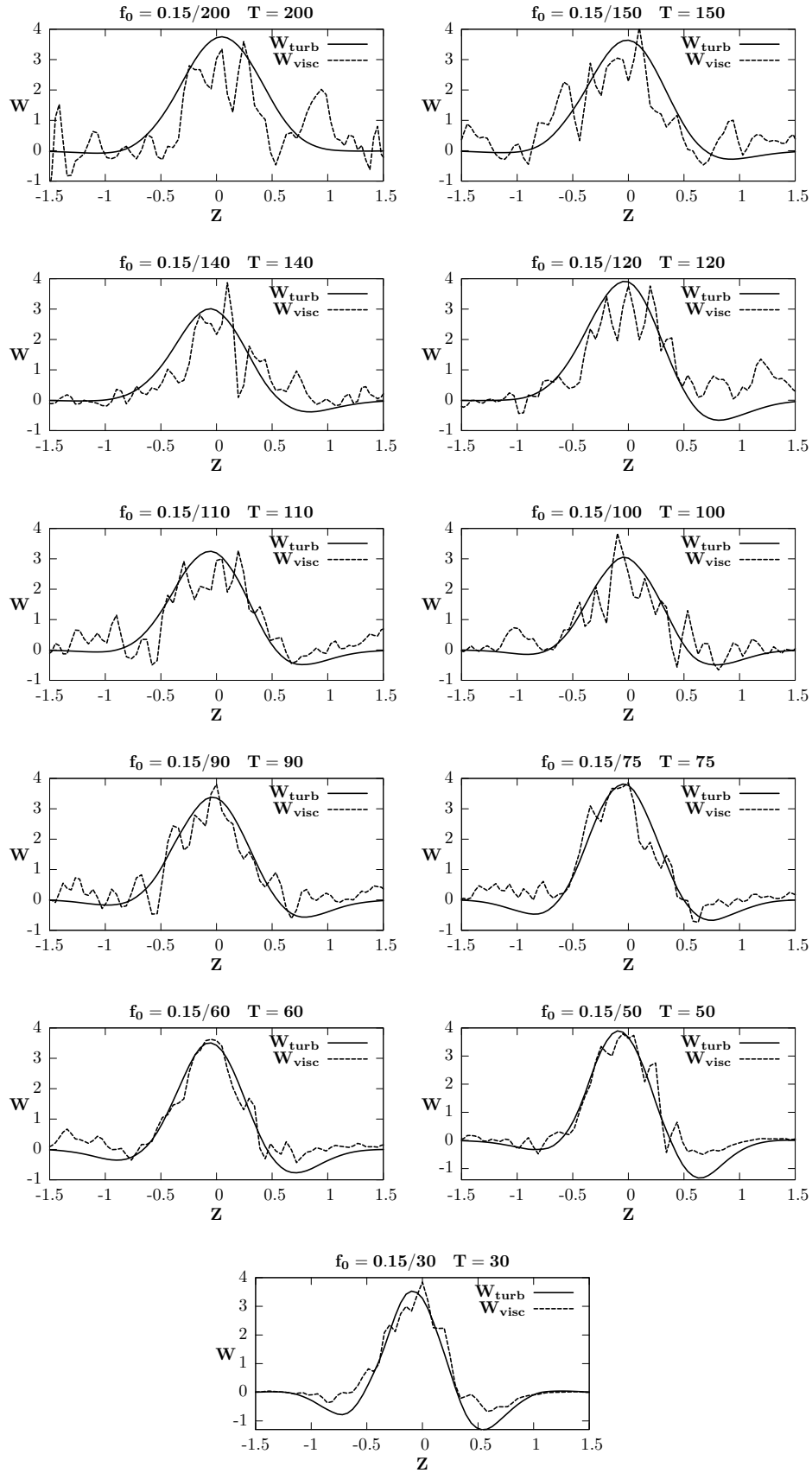


Figure 7: The least squares fit between  $W_{turb}$  (solid curves) and  $W_{visc}$  (dashed curves) for all of the weak forcing cases.

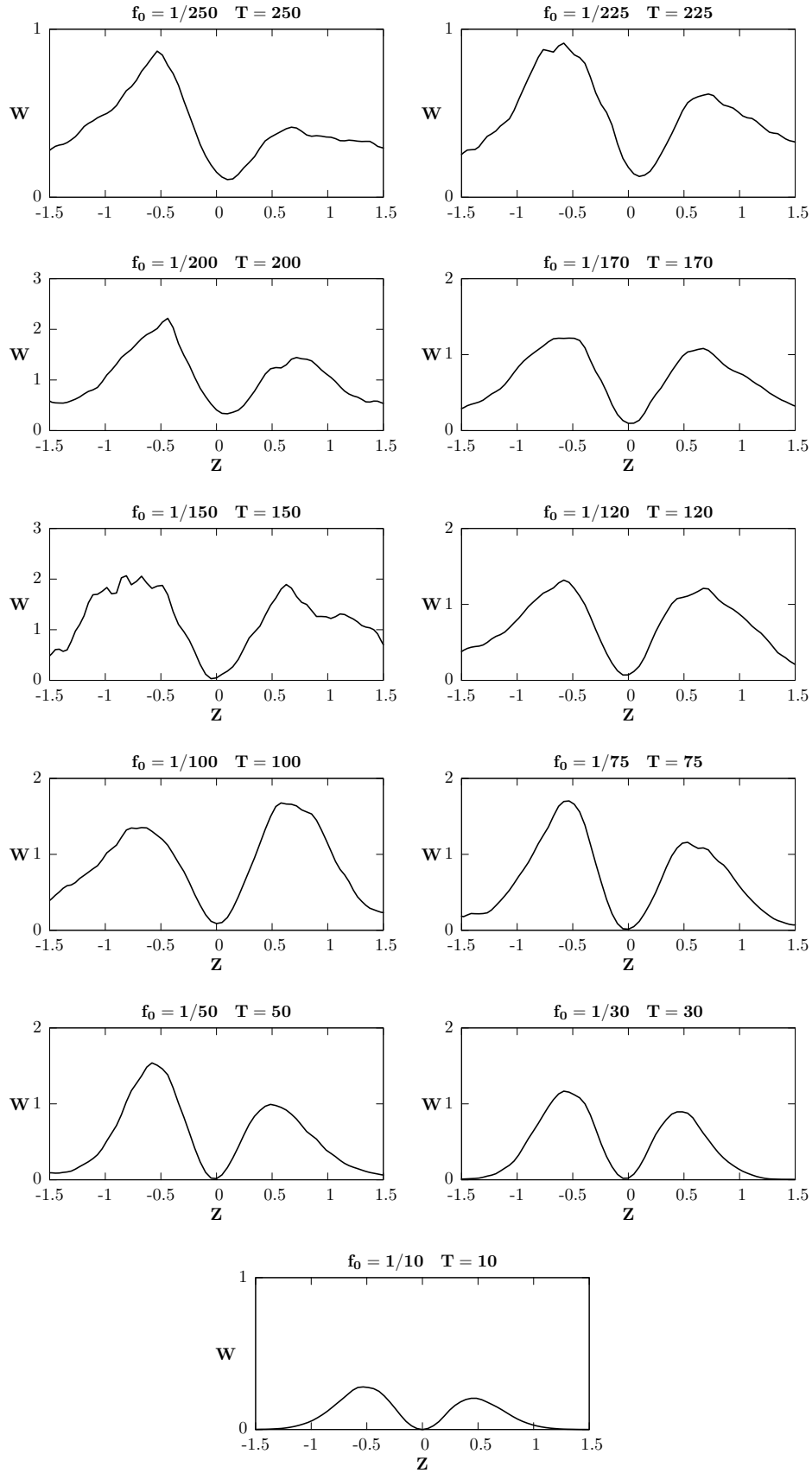


Figure 8: The energy dissipation rate due to the effective viscosity at each depth for the same strong forcing cases as in fig. 6.

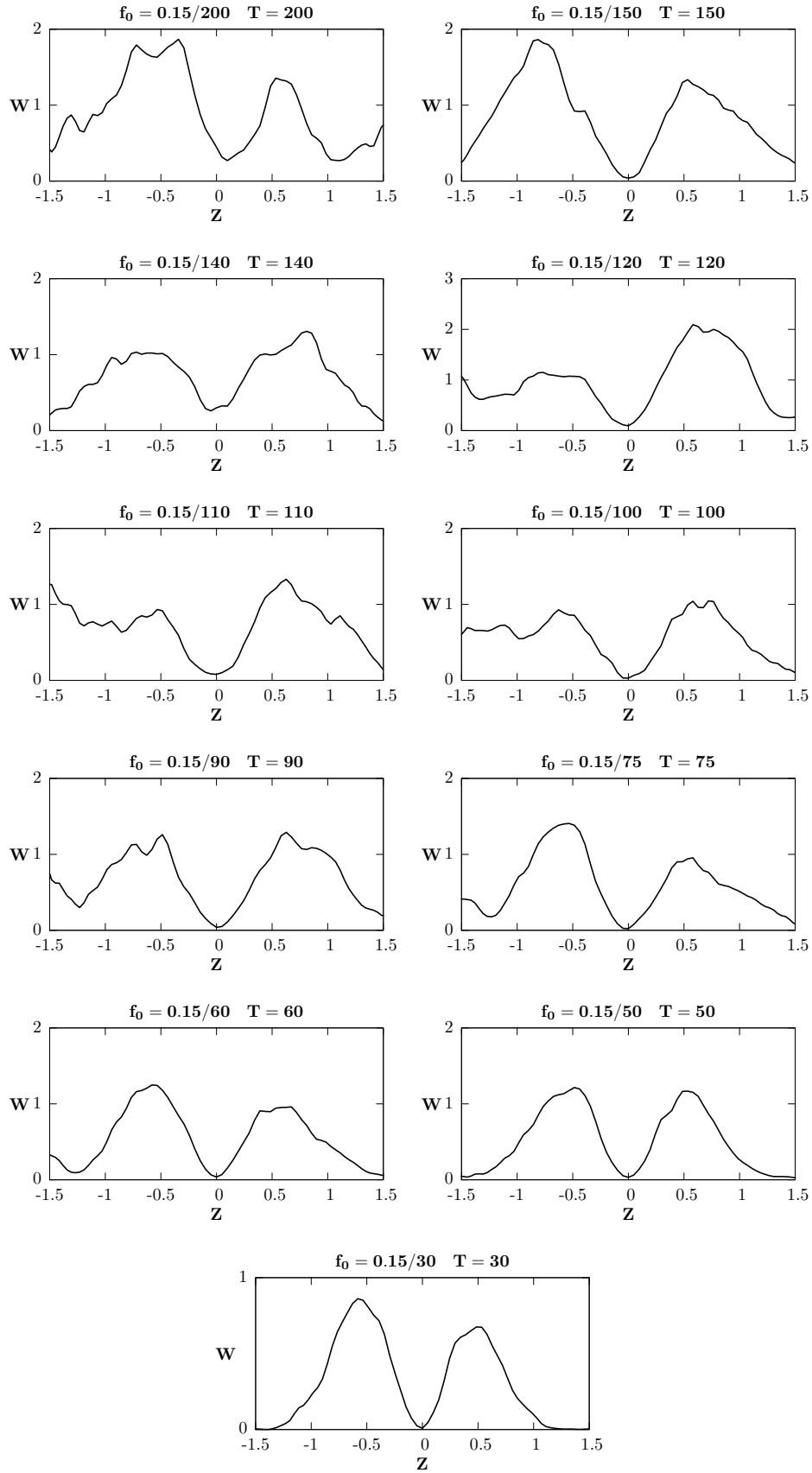


Figure 9: The energy dissipation rate due to the effective viscosity at each depth for the weak forcing cases.

	Depth Fit (sec. 3.2.1)		Dissipation Match (sec. 3.2.2)	
	slope	zero intercept	slope	zero intercept
strong forcing	$2.6 \pm 0.5$	$3.0 \pm 0.2$	$2.6 \pm 0.4$	$2.4 \pm 0.1$
weak forcing	$2.1 \pm 0.4$	$2.4 \pm 0.2$	$3.1 \pm 0.4$	$0.9 \pm 0.2$

Table 2: The linear regression parameters corresponding to the solid and dashed lines in fig. 10.

The curves in the figure correspond to the perturbative expansion and the points correspond to the direct calculation. Since the perturbative calculation assumes that the forcing period is small compared to the convective turnover time we have used a solid line only for smaller periods. For the longer periods (dotted line) this method is no longer applicable.

The error bars in the top plot of fig. 10 correspond to the standard deviation of  $\nu_0$  as derived from the least squares fitting procedure. These error bars capture only the variations introduced from turbulent eddies with periods shorter than the forcing period. Variations due to eddies with longer turnover times appear as systematic errors. This explains why the error bars grow from left to right, and why the scatter of the points with low periods is much larger than their formal error bars.

We see that the effective viscosity predicted with all three methods scales linearly with the forcing period, and the two direct calculations with strong forcing show that the effective viscosity saturates at  $T \approx 2\tau$ , after which it remains roughly constant. One physically expects to see this saturation, because for forcing periods much larger than any convective timescales there is no reason why the dissipation efficiency of the convective zone should depend on the period.

We do not see the saturation in the weak forcing case, because there are no points at long enough perturbation periods. The reason for this is that longer forcing period simulations require more time steps in order to achieve acceptable fits, hence they become extremely time consuming to compute in the weak forcing case. We also do not see the saturation for the perturbative calculation, because it is due to the neglected higher order terms.

In order to obtain a functional dependence for the effective viscosity on period we perform a least square linear fit to the points in the range  $0.3\tau < T < 1.5\tau$ , where linear scaling is seen to apply. The resulting fits are shown in fig. 10 as solid lines for the weak forcing case and dashed lines for the strong forcing case. The parameters of the fitted lines are given in table 2. This also allows us to get an estimate of the error bars associated with each point. Those are shown in the upper left corners of the plots in fig. 10.

### 3.3.1. Amplitude Dependence

The three dependences in fig. 10 and correspond to three different forcing strengths: strong forcing with  $v_{forc}/v_{conv} \approx 2.7$ , weak forcing with  $v_{forc}/v_{conv} \approx 0.4$  and the perturbative calculation with  $v_{forc}/v_{conv} \ll 1$ , where  $v_{forc}$  is the peak velocity due to the external forcing and  $v_{conv}$  is the root mean square velocity for the central plane of the box in the absence of forcing. This allows

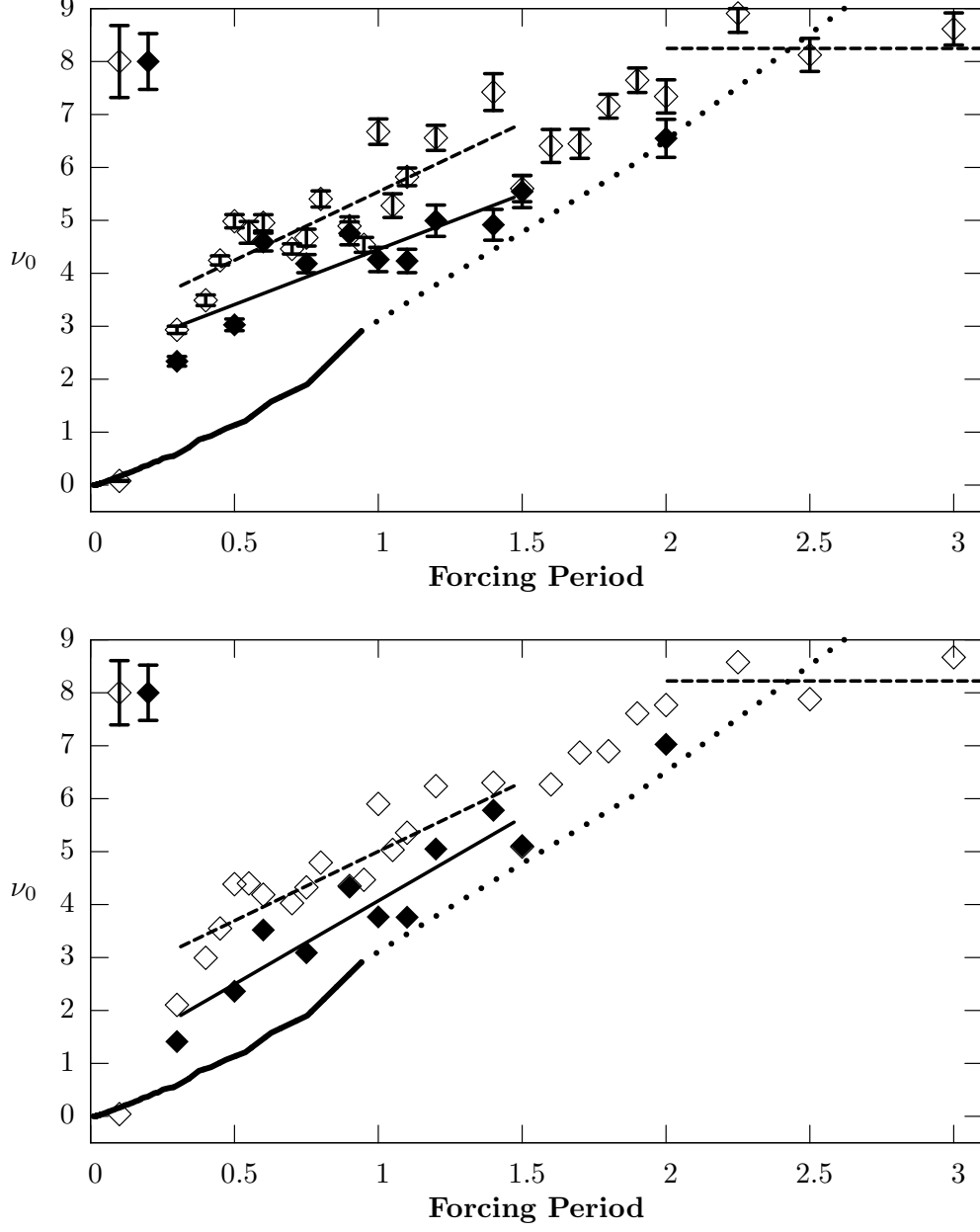


Figure 10: Comparison between the after-the-fact perturbatively estimated viscosity (curve) and the viscosity obtained from the direct simulations by least squares fit of  $W_{visc}$  (eq. 10) to  $W_{turb}$  (eq. 8) : left; and from setting  $\int W_{turb}(z) = \int \widetilde{W}_{visc}(z)$ . The strong forcing points are plotted with empty symbols, and the weak forcing with filled symbols. The horizontal axis is the perturbation period ( $T$ ) in units of the convective turnover time in the box and the vertical axis is the value of the scaling constant  $\nu_0$  (eq. 11). The error bars of the points on the top plot correspond to the standard deviation of  $\nu_0$  obtained from the least square fitting procedure. Also shown are linear least square fits to the strong forcing points (dashed line) and the weak forcing points (solid line) as well as an estimate of the maximum effective viscosity for the strong forcing case.

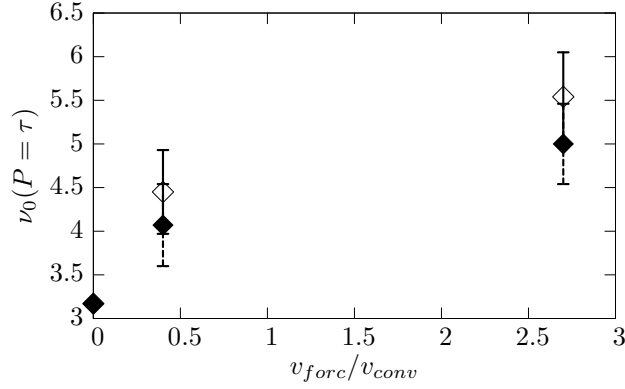


Figure 11: The dependence of the effective viscosity on the forcing strength. The symbols correspond to the effective viscosity estimation described in section 3.2.2 (filled) and section 3.2.1 (empty)

us to look at the dependence of the effective viscosity on forcing amplitude. In fig. 11 we plot our best estimates for the values of the effective viscosity when the external forcing period corresponds to the convective turnover time as a function of  $v_{forc}/v_{conv}$ . The values and their error bars for the direct calculations were obtained by evaluating the linear fits from figure 10 at  $T = \tau$ .

Clearly the effective viscosity is larger for larger external forcing. From the perturbative calculation we know that for  $v_{forc} \ll v_{conv}$ , the effective viscosity is independent of the forcing amplitude. Also we expect that for very large amplitudes the shear due to the external forcing will be large enough to be the dominant source of turbulence in the system. At that point the presence of the convection become immaterial and the numerical code we are using is not ideally suited for simulating the flow in this regime.

#### 4. Conclusions

We have completed a set of simulations of turbulent convection relevant to stellar surface convective zones with external forcing introduced directly in the momentum equation, in the form of a periodic horizontal height dependent gravitational acceleration. We then found an effective viscosity assumed to be of the form of eq. 11 (in accordance with mixing length theory), using two methods:

1. least squares fitting of the work done by the external forcing on the flow at each height to the energy transported or dissipated away from that height by the effective viscosity.
2. matching the overall energy deposited into the box by the external forcing to the energy dissipated by the effective viscosity.

We found that these two methods give consistent results and the one parameter fits of the first method were able to capture the details of the observed height dependence (see fig. 6 and 7), which suggests that the effective viscosity assumption for treating turbulent dissipation in convective zones is valid.

Further we compared this directly obtained effective viscosity with the lowest order perturbative expansion of Goodman & Oh (1997) applied to the steady state flow without forcing and we see that the values, this much less computationally intensive approach produces, are within a factor of two of the directly obtained values. The differences seen are easily explained by the fact that the perturbative expansion is valid for the case when the velocities caused by the external forcing are small compared to the turbulent velocities, however currently it is not practical to simulate this case, and we were forced to use external forcing that at best produced velocities of the same order of magnitude as the turbulent velocities in the box.

Finally both of the above methods based on the output of numerical simulations produce roughly linear scaling of effective viscosity with the period of the external forcing and they both predict significantly larger dissipation than what Zahn (1966, 1989) proposes based on the assumption of Kolmogorov turbulence.

Our conclusion is that for forcing periods comparable to the local turnover time of the largest eddies ( $\tau$ ) the effective viscosity scales linearly with period and for our convective box its  $x, z$  component can be approximated by:

$$\nu_{x,z}(T) \approx 3 < v_z^2 >^{1/2} H_p \min \left[ \frac{T}{2\tau}, 1 \right] \quad (14)$$

Where  $T$  is the period of the external forcing.

The limited spatial resolution of our box does not allow us to reliably simulate the case of  $T \ll \tau$ . In that regime the assumptions for Kolmogorov turbulence hold and the effective viscosity should scale quadratically with the period (Goodman & Oh, 1997).

The effective viscosity given by eq. 14 is approximately a factor of two larger than the corresponding effective viscosity component in Penev et al. (2008b), even though both values are based on the same perturbative calculation. This is expected since, if we were to define a mixing length parameter for the convective box used in this paper, its value would be  $\alpha \approx 3$ . This is approximately a factor of two larger than the mixing length parameter usually assumed for the Sun and relevant to the convective simulations used in deriving the Penev et al. (2008b) result.

The viscosity of eq. 14 has exactly the form of the Zahn (1966, 1989) prescription including the saturation period. This might be the resolution of the apparent discrepancy between the dissipation necessary to explain tidal circularization and the red edge of the Cepheid instability strip on one hand and the observed amplitudes of the solar p-modes on the other. For small periods (of order minutes) the Kolmogorov scaling of turbulence holds and a quadratic decrease in the effective viscosity is appropriate. For long periods (of order days) the assumptions necessary for Kolmogorov cascade are not satisfied and the effective viscosity is found to scale linearly with period.

The only difference between eq. 14 and Zahn's prescriptions is that, even after correcting for the unnaturally high value of  $\alpha$  in our simulations, our prescribed viscosity is significantly larger. This is hopeful, since a larger viscosity is necessary in order to explain the Meibom & Mathieu (2005) results of observed main sequence circularization. Whether our prescription is large

enough to be consistent with those observations, while not too large to be inconsistent with other observational constraints remains to be verified.

## References

- Goldreich, P. & Keeley, D. A. 1977, *ApJ*, 211, 934
- Goldreich, P. & Kumar, P. 1988, *ApJ*, 326, 462
- Goldreich, P., Murray, N., & Kumar, P. 1994, *ApJ*, 424, 466
- Goldreich, P. & Nicholson, P. D. 1977, *Icarus*, 30, 301
- Gonczi, G. 1982, *A&A*, 110, 1
- Goodman, J. & Oh, S. P. 1997, *ApJ*, 486, 403
- Malagoli, A., Cattaneo, F., & Brummell, N. H. 1990, *apjl*, 361, L33
- Meibom, S. & Mathieu, R. D. 2005, *ApJ*, 620, 970
- Penev, K., Barranco, J., & Sasselov, D. 2008a, *ArXiv e-prints*
- Penev, K., Sasselov, D., Robinson, F., & Demarque, P. 2007, *ApJ*, 655, 1166
- . 2008b, *ArXiv e-prints*
- Robinson, F. J., Demarque, P., Li, L. H., Sofia, S., Kim, Y.-C., Chan, K. L., & Guenther, D. B. 2003, *MNRAS*, 340, 923
- Sofia, S. & Chan, K. L. 1984, *apj*, 282, 550
- Stein, R. F. & Nordlund, A. 1989, *ApJ*, 342, L95
- Verbunt, F. & Phinney, E. S. 1995, *A&A*, 296, 709
- Zahn, J. P. 1966, *Ann. d’Astrophys.*, 29, 489
- Zahn, J. P. 1989, *A&A*, 220, 112